Wavelet Energy Entropy Unit Protection by Fault Condition Information Fusion

Zhenwei Guo, Ruiqiang Zhao*, Haojie Li, Yongyan Jiang, Weiyong Ma

Abstract—**Transient protection has of a line from the head fault of the adjacent line. To solve these problems, wavelet energy entropy of fault high-frequency current is used as original fault characteristic. Initial fault Angle and transition resistance are defined as two fault condition attributes of fault characteristics. The inline relationship between fault characteristics and fault condition attributes is mined, and the fault characteristics and fault condition attributes are fused to obtain the synthetic fault characteristics containing fault attribute information. The fault characteristics are used to differentiate external faults from internal faults, and the fault direction is used to distinguish bus faults from line faults. The algorithm overcomes the adverse effects of fault condition attributes, improves the protection reliability, and can protect both a line and a bus. The algorithm solves 42.2% of cross data, 41.6% of false actions or 8.9% of rejected actions. Lots of ATP/EMTP simulation experiments validate that the algorithm can accurately judge faults under various fault conditions.**

Index Terms—**Transient unit protection; Wavelet energy entropy; Synthetic fault characteristics; Information fusion; Fault condition attribute.**

I. Introduction

The scale and complexity of the contemporary power system have increased recently due to the widespread use of ultra-high-voltage transmission technology. This has placed higher demands on the speed and responsiveness of power system protection [1], [2], [3]. Providing faster fault detection and protection solutions can enhance the stability and reliability of the power system, bolster public safety, and increase the transmission efficiency and capacity of transmission lines for power transmission [4]. Conventional protection schemes based on power frequency measurements suffer from significant time delays in operation and are susceptible to fluctuations in the power system load, rendering them inadequate for meeting the ultra-high-speed operational requirements of modern power grids [5] [6]. The instantaneous voltage and current in the power system that are caused by faults are referred to as transient elements, encompassing information about the nature, location, duration, and other aspects of the fault. Compared to protection schemes based on power frequency measurements, transient protection is garnering increasing attention due to its inherent speed advantages [7].

Research of transient protection has made a lot of progress in various aspects. The ratio of forward and backward traveling wave amplitude was used to construct an internal and external fault identification method [8]. Reference [9] proposes a protection technology that uses wavelet coefficients to detect faults, which is greatly affected by data-window's length. Rapid protection is realized by the time when traveling wave first arrival at two ends of the transmission line [10]. Reference [11] proposes a line protection algorithm basing on voltage and current traveling wave polarity. For the poor transient-response of capacitor voltage transformers, it is difficult to purify voltage travelling wave under some conditions. To overcome this shortcoming, reference [12] proposed a protection technology that utilizes the current traveling-wave's polarity and the direction of the modal component of the voltage before the fault, but this method is only applicable to the fault type with small voltage signal changes. Reference [13] proposed for the first time a protection scheme using both ends of the line to attenuate DC component information, but ensuring information synchronization at both ends is an arduous challenge for this method. HHT is used to calculate instantaneous amplitude of the first current traveling-wave to be distinct between bus fault from line fault [14] [15]. However, HHT algorithm is prone to mode aliasing, and its anti-interference ability needs to be improved. Reference [16] proposes a transient protection scheme suitable for transmission lines containing UPFC, but this scheme needs to detect the fault characteristic quantity of all lines connected with the bus bar, and the operation is complicated. Reference [17] introduces the non-cellular traveling-wave protection scheme, but this method cannot achieve 100%-line protection. Reference [18] points out that the fault characteristic value when the initial fault Angle is -5° is 10% of the value when the start fault angle is 90°. The protection sensitivity can't meet the requirements, and the smaller the start fault angle, the lower the protection sensitivity. When initial phase Angle is within 18° before and after the zero crossing, its protection reliability cannot meet the requirements. Wavelet singular entropy and wavelet energy entropy were used to construct

Manuscript received December 18, 2024; revised December 19, 2024.

This work was supported by the National Natural Science Foundation of China under Grant 52067005, and the Guangxi Natural Science Foundation under Grant number 2021GXNSFAA220061.

ZhenWei Gou is an associate professor of the School of Electrical and Mechanical Engineering, Guilin University of Electronic Science and Technology, Guilin 541004, China. (e-mail: gzwcbf@sina.com).

RuiQiang Zhao is a postgraduate student of School of Electrical and Mechanical Engineering, Guilin University of Electronic Science and Technology, Guilin 541004, China. (corresponding author to provide e-mail: 3295657367@qq.com).

Haojie Li is a postgraduate student of School of Electrical and Mechanical Engineering, Guilin University of Electronic Science and Technology, Guilin 541004, China. (e-mail: 798225917@qq.com).

YongYan Jiang is a postgraduate student of School of Electrical and Mechanical Engineering, Guilin University of Electronic Science and Technology, Guilin 541004, China. (e-mail: 1583196429@qq.com).

WeiYong Ma is an associate professor of the School of Electrical and Mechanical Engineering, Guilin University of Electronic Science and Technology, Guilin 541004, China. (e-mail: 2261664936@qq.com).

the protection criterion, but ignores the effect of the initial fault angle on the algorithm [19].

If there is an external fault, fault traveling wave passes through the bus and then arrives at the detection device location, and high-frequency components of transient current attenuates a large amount [19]. When the fault locates inside the zone, fault traveling-wave reaches detection device location directly, and high-frequency signal of the transient current does not change significantly. There is a significant difference between the high-frequency components of faults in and out of the region. The Shannon entropy can represent the component information of fault transient signal well. In the article, wavelet transform extracts the fault high-frequency current signal, and energy entropy of the fault high-frequency current component is calculated as an original fault feature. The start fault angle and transition resistance are defined as fault condition attributes. And using information fusion technology, the fault condition attributes and fault characteristics are fused to obtain synthetic fault characteristics. The fault is determined by synthetic fault characteristics, and the adverse effects of fault initial Angle and transition resistance are overcome. The method's effectiveness is verified by lots of ATP/EMTP simulation experiments.

II. Wavelet Energy Entropy

Wavelet-transform is a commonly used non-stationary signal processing technology in multiresolution analysis, which has good time-frequency analysis function and can provide well localized information in time and frequency [20], [21].

Compared with continuous wavelet-transform, discrete wavelet-transform discretizes the scale-factor, a, and the shift factor, b, which greatly reduces the computation amount. The core idea of Mallet discrete wavelet transform is to decompose the signal by orthogonal wavelet basis. That is, the time series x(n) is decomposed into high-frequency detail d_1 and low-frequency approximate a_1 in the frequency domain, and then the low-frequency signal a_1 is decomposed continuously foe multi-resolution signal [22]. Wavelet-transform constructed by db4 wavelet basis function has high resolution to high-frequency signals, and it is selected to process the transient current and voltage signals in this paper.

Information entropy can reflect the complexity and sequence uncertainty of signals. Information entropy is used to mine information from large amounts of data [23]. signal's uncertainty and complexity can be reflected in the wavelet energy entropy. The higher the energy and the more uniform the probability distribution of the signal, the larger the wavelet energy entropy. Therefore, the Shannon entropy of fault current wave can reflect the change of current before and after fault and is suitable for fault characteristics. High-frequency fault current can reflect the transient characteristics of fault more. After wavelet transform decomposes the fault current, the Shannon entropy of the high-frequency current is calculated to obtain the energy entropy of wavelet transform, which is used as the fault characteristic.

The square of wavelet reconstruction coefficients of each frequency band in the time-window is selected as the wavelet-energy per scale. In a certain time window, total energy of signal x equals the sum of the wavelet energies on each frequency band. By combining it with the Shannon entropy, wavelet energy entropy *WEE* is deduced, and its corresponding formula (1) is shown as following [23].

$$E_j = \sum_j \left| D_j(k) \right|^2$$
$$E = \sum_j E_j \tag{1}$$
$$WEE = -\sum_j \left(\frac{E_j}{E} \right) ln \left(\frac{E_j}{E} \right)$$

Where, $D_j(k)$ is a reconstruction coefficient of wavelet corresponding to a sampling point in the j band; E_j is the wavelet-energy per frequency band; E is total energy of signal x, and *WEE* is the wavelet energy entropy in the time window for sampling.

III. The Proposed Algorithm Principle

Typical 500kV transmission line structure is shown in Fig. 1. The relay is installed at the first end of Line 3. Bus B and line 3 are the protected object. Define the positive direction is from bus bar B to line 3, and the direction from line 3 to bus B is defined as negative. When the Relay determines that line 3 or bus B are faulty, the circuit breaker CB_1 trips.

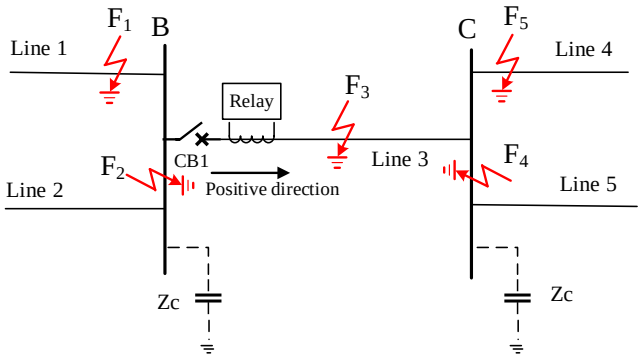

Fig. 1. Schematic diagram of 500kV transmission system.

A. Transient Traveling Wave Busbar Propagation Characteristics

The impedance Z_C of bus-to-ground distributed capacitance in Fig 2 is a frequency variable parameter. Its impedance value changes with frequency, while the impedance of the transmission line remains basically unchanged, which results in wave impedance to be discontinuous at bus bar. The traveling wave propagation path on bus bar is shown in Fig. 2(a), and the incident traveling wave U_{L1} reflects and folds at the bus bar. U_{L2} is a refracted traveling-wave and U_{L1R} is a reflected traveling wave. It is assumed that the transmission line is infinitely long. By Petersen's rule, the equivalent circuit with lumped parameter shown in Fig. 2 (b) is obtained [24]. According to the circuit model in Fig. 2 (b), the refracted wave U_{L2} can be deduced.

$$U_{L2} = H(s) U_{L1} = \frac{2(Z_C \parallel Z_{L2})}{(Z_C \parallel Z_{L2}) + Z_{L1}} U_{L1} \tag{2}$$

Where, $H(s)$ is the transfer function of the bus's equivalent capacitance to earth. That is, the refraction ratio. By replacing s with $j\omega$, Refraction Coeff. $H(\omega)$ of the busbar's equivalent capacitance to ground in the frequency domain can be obtained.

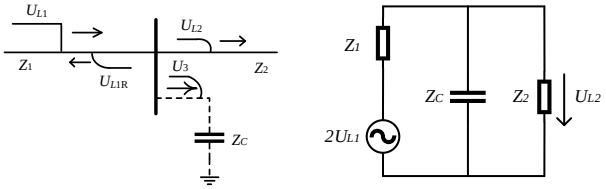

(a) Traveling wave passing path (b) Equivalence circuit

Fig. 2. Fault traveling wave propagation through bus.

The frequency characteristics of Z_C when the distributed capacitance C to earth is 2000pF, 6000pF, 10000pF, 50000pF and 0.01μF are studied below. The transmission line impedance Z_1 and Z_2 are set to 300Ω. By substituting the above data into the formula (2), the amplitude-frequency characteristic curve of the bus's equivalent capacitance to ground is obtained, as shown in Fig. 3.

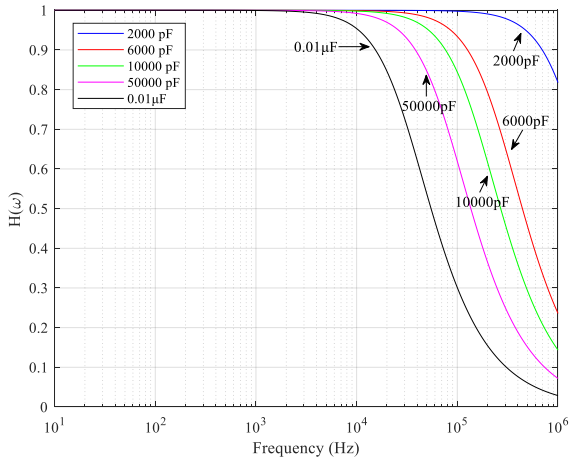

Fig. 3. Amplitude-frequency characteristics of bus equivalent capacitance to ground.

It is clearly from Fig. 3 that the bus-to-ground distributed capacitance impacts a remarkable attenuating influence on the high-frequency (above 50 kHz) transient component, but has a little effect on the low-frequency (below 10 kHz) transient component. It can be inferred that when a fault occurs outside zone, fault transient high-frequency signal will attenuate greatly at the bus bar before entering the protected zone. When a fault occurs inner zone, fault signal does not pass through the bus, and fault high-frequency component does not change significantly. Therefore, a transient protection method can be constructed according to the difference of transient high-frequency components between regional faults and external faults.

B. Basic Principle of Fault Determination by Wavelet Energy Entropy

According to analysis in Section 2.1, transient high-frequency components of internal fault are obviously different from those of external fault due to the effect of bus-ground distribution capacitance, and wavelet energy entropy can reflect this difference. Hence, internal fault or external fault is discerned by detecting the wavelet energy entropy of transient high-frequency signals.

In Fig. 1, when internal bus B happens fault, fault traveling-wave propagates from bus B to line 3, and fault direction is positive. The detected wavelet energy entropy is very large because the busbar capacitance does not attenuate the fault traveling wave. When internal line 3 is faulty, fault traveling wave passes directly to Relay. The fault direction is negative. The propagation path also has no attenuation effect of bus capacitance. so wavelet energy entropy is also large.

When external line 1 or line 2 are fault, fault traveling wave passes through bus B before reaching the Relay detection device. Because of the attenuation of bus bar B distribution capacitance, the detected wavelet energy entropy is small. Similarly, when external line 4 or line 5 are faulty, fault traveling wave passes through bus C before reaching the Relay detection device, and the detected wavelet energy entropy is also small.

To sum up, when faults occur in the protected area, wavelet energy entropy value is large. If a fault happens outside zone, wavelet energy entropy value is small. If a fault happens on bus B, fault direction is positive. When line BC is faulty, the fault direction is negative. This makes it possible to distinguish between internal and external faults by wavelet energy entropy. When it is determined that the fault is internal, fault direction is used to further distinguish bus B fault from line 3 fault.

C. Fault Direction Identification

The fault direction can be identified quickly by using the ratio of the forward and reverse amplitude integrals. As shown in formula (3), signals I^- and I^+ represent the integration of backward wave i^- and forward wave i^+ over the period $[t, t + dt]$ [25].

$$I^+ = \int_t^{t+\frac{2d_{\min}}{v}} i^+(t)\,dt$$
$$I^- = \int_t^{t+\frac{2d_{\min}}{v}} i^-(t)\,dt \tag{3}$$

Where, t denotes the time when fault traveling wave first arrives at the detection element. Setting an appropriate time dt constant, such as $dt \leqslant 2d_{min}/v$, d_{min} represents the length of the shortest line connected with busbar B, which can eliminate the effect of refracted and reflected waves from other lines. Fault direction discrimination coefficient K is defined, as shown in formula (4).

$$K = \frac{I^+}{I^-} \tag{4}$$

If coefficient K is greater than the threshold K_{set} ($0<K_{set}<1.5$), fault direction is positive; otherwise, fault direction is negative.

D. Fault Condition Attributes Affect Reliability Analysis

In the grid system shown in Fig. 1, multiple fault points are set, including F_1 point of line 1, which is 1km away from bus B; F_2 point on bus B; F_3 of Line 3, 1km away from bus C; F_4 point on bus C; F_5 of Line 4, 1km from bus C. Wavelet energy entropy (*WEE*) of high-frequency component of [50kHz,100kHz] is taken as the research object. TABLE I

shows *WEE* of F_3 point and F_5 point with different fault condition attributes. Under different fault condition attributes, the value ranges of *WEE* for internal fault and *WEE* for external fault are interleaved. For example, *WEE* (0.1639, 0Ω and 5°) of internal F_3 point is less than *WEE* (0.2337, 0Ω and 90°) of F_5 point.

TABLE I
WEE OF F_3 POINT FAULT AND F_5 POINT FAULT WITH DIFFERENT FAULT CONDITION ATTRIBUTES

θ_f(°)	R_f(Ω)			
	0	10	100	250
Internal F_3 point fault (1 km from bus C)				
1	0.0095	0.0087	0.0048	0.0024
3	0.0648	0.0600	0.0334	0.0167
5	0.1639	0.1517	0.0848	0.0427
45	6.5707	6.1030	3.5087	1.8192
85	11.7574	10.9330	6.3359	3.3120
90	11.8318	11.0023	6.3766	3.3336
External F_5 point failure (1 km from bus C)				
1	0.0002	0.0001	0.0001	0.0000
3	0.0010	0.0010	0.0005	0.0003
5	0.0027	0.0025	0.0014	0.0007
45	0.1249	0.1160	0.0665	0.0340
85	0.2321	0.2158	0.1241	0.0637
90	0.2337	0.2173	0.1249	0.0642

It is assumed that faults with different fault condition attributes occur with equal probability. For the sake of simplicity, first analyze the gold attribute fault in Table I. 37.4% data of F_3 points and F_5 points are crossed. If all the faults of line 3 are activated, 38.9% faults of line 4 will be disactivated. If all faults of line 4 are not mis-activated, then within a total range of 12° near the zero crossing of the initial phase Angle, when line 3 fails, the protection will refuse to act, and the rejection action rate is 6.7%. WEE under various fault condition attributes is shown in Fig. 4. FA indicates the start fault angle, and FR indicates the fault resistance. Considering all fault conditions, the error rate and rejection rate will be higher. If the protection action value is set directly according to *WEE*, in any case, it can't meet the requirements of internal fault reliable action and external fault reliable no action at the same time. This seriously affects the reliability of protection.

Fault condition attributes also significantly affect the *WEE* of the same fault point. For example, if F_3 point is faulty, when R_f = 0Ω, the *WEE* (11.8318) at 90° θ_f is 1245 times the *WEE* (0.0095) at 1° θ_f. If the protection action value is set directly according to these *WEE*, the protection sensitivity can't meet the requirements in the case of weak faults. Therefore, these problems must be solved.

The inline relationship between *WEE* and fault condition attributes is explored from Fig. 4. *WEE* changes with the initial fault Angle FA (0°~180°), and presents the characteristics of approximately half-sinusoidal waveform change. *WEE* is symmetric about FA=90°. *WEE* changes with the change of fault resistance FR, showing a trend of attenuation index. Lots of fault simulations reveal that the *WEE* value of 180°~360° is almost the same as the *WEE* value of 0°~180°. That is, when FA is 0°~360°, *WEE* is symmetric about FA=180°.

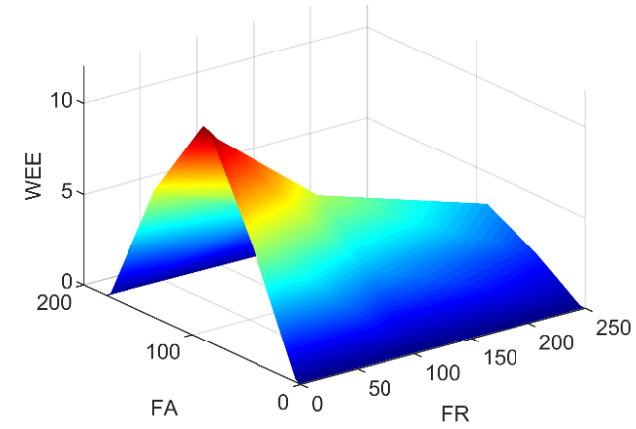

(a) Point F_3 fault 1 km from bus C

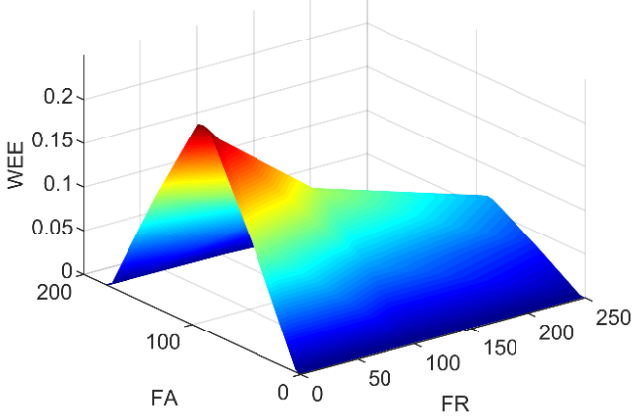

(b) Point F_5 fault 1 km from bus C

Fig. 4. *WEE* and fault condition attributes.

E. Fault Information Fusion Protection Algorithm

It is found that initial fault phase Angle and transition resistance are two key factors affecting *WEE*. They are therefore defined as two fault condition attributes of *WEE*. Information fusion technology is used to fuse fault condition attribute information into *WEE* to generate synthetic fault characteristics *NWEE*. *NWEE* endowed with the two fault conditions becomes the four-dimensional data with multiple information of time, initial fault phase angle, transition resistance and fault characteristics. Judging the fault by *NWEE* is equivalent to examining the fault characteristics from the perspective of their fault condition attributes. This method greatly improves the accuracy of fault diagnosis and protection reliability.

The process of the protection algorithm is shown in Fig. 5.

Step 1, collect voltage and current signals from line 3.

Step 2, wavelet transform is used to extract high-frequency signals from the fault current, and *WEE* of fault current is calculated.

Step 3, calculate start fault Angle θ_f and fault resistance R_f.

Step 4, the information fusion method shown in formula (5) is used to fuse Angle θ_f and transition resistance R_f to *WEE* to generate comprehensive fault feature *NWEE*.

Step 5, if *NWEE* > Aset, it is identified as an internal fault; otherwise, external fault. Aset is the setting value of the protection action.

Step 6, identify the fault direction.

Step 7, if positive, it indicates Line 3 fault, if not, bus B fault.

Step 8, circuit breaker CB_1 disconnects.

$$\begin{cases} NWEE = f(\theta_f, R_f) * WEE \\ f(\theta_f, R_f) = k * \left(\left(1 + \cos\left(a * \theta_f\right)\right) * \left(e^{b*R_f} + c * e^{d*R_f}\right) \right)^{-1} \end{cases} \quad (5)$$

Where, k is the comprehensive fault characteristic adjustment constant, a, b, c, d is the fault information fusion constant, R_f transition resistance, and θ_f is the initial fault Angle.

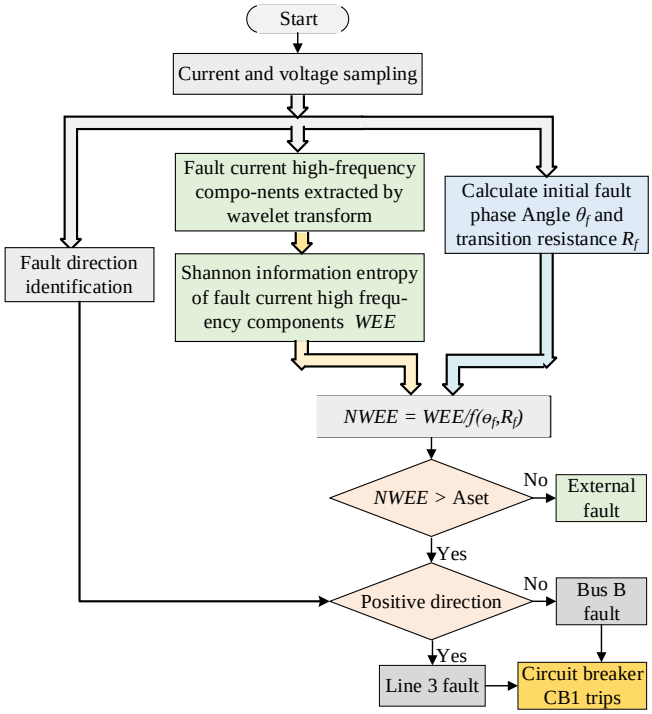

Fig. 5. Flowchart of the fault information fusion protection algorithm.

IV. Simulation Example Verification

With reference to China Southern Power Grid, the 500kV transmission system model built with ATP/EMTP is shown in Fig. 6. The protection device is at first end of line BC. It protects transmission line BC and bus bar B. Specified that the direction from bus B to line BC is positive. The length of the AB, BC and CD lines is 155km, 180km and 175km respectively. The capacity of power source S_1, S_2, S_3 and S_4 is 18GVA, 15GVA, 10GVA and 20GVA respectively. The equivalent capacitance C of the bus to ground are set to 0.01μF. The sampling frequency is set to 400kHz.

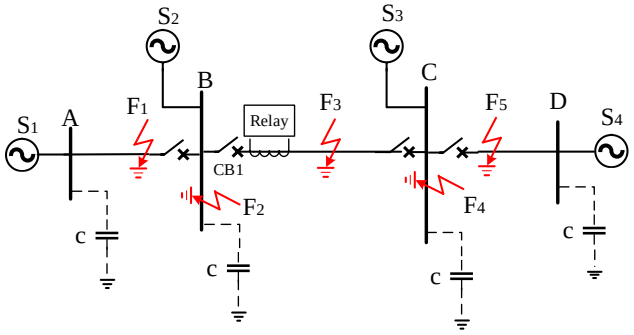

Fig. 6. Structure diagram of simulation experiment system.

In the power grid model shown in Fig 6, F_1 fault points, F_2 fault points, F_3 fault points, F_4 fault points and F_5 fault points are respectively set in line AB, bus B, line BC, bus C and line CD. Initial fault Angle $\theta_f \in [0°, 90°]$, transition resistance $R_f \in [0\Omega, 250\Omega]$. According to Section 3.4.1, between 0° and 360°, *WEE* is symmetric with respect to FA=180°; Between 0° and 180°, *WEE* is symmetric about FA=90°. Therefore, due to limited space, the following experimental simulation only lists part of the content between 0° and 90°.

A. Outside Line AB Fault

When a phase A ground fault is at the point F_1 of external line AB, fault current traveling wave spreads through bus B to the protection installation. Direction of fault detected by Relay is positive. The distance L1 from the point F_1 of line AB to bus B is 1km and 154km respectively. When F_1 point is faulty with $R_f = 50\Omega$, $\theta_f = 45°$, *NWEE* is shown in Fig. 7. It is easy to see from Fig. 7 that at the moment of fault, the *NWEE* increases steeply, which indicates that there is a fault occurring in the system, and the fault characteristics are obvious.

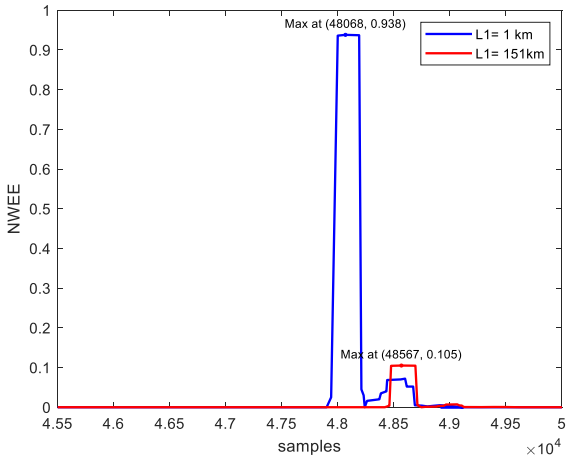

Fig. 7. *NWEE* for line AB fault.

The *NWEE* at point F_1 fault with different fault condition attributes is shown in TABLE II. For L1=1km, the *NWEE* is at [0.3669, 1.2239] and the maximum value is 3.3 times the minimum value. For L1=154km, the *NWEE* is at [0.0478, 0.1536] and the maximum value is 3.2 times the minimum value. *NWEE* for all faults is at [0.0478, 1.2239] for line AB faults.

TABLE II
NWEE FOR F_1 POINT FAULT

θ_f(°)	R_f(Ω)			
	0	50	100	250
		L1=1km		
1	0.3669	0.4182	0.4580	0.4968
3	0.5870	0.6708	0.7362	0.8022
5	0.6910	0.7907	0.8689	0.9495
45	0.8126	0.9388	1.0395	1.1551
90	0.8539	0.9888	1.0970	1.2239
		L1=174km		
1	0.0478	0.0533	0.0583	0.0621
3	0.0734	0.0838	0.0930	0.1003
5	0.0863	0.0988	0.1086	0.1187
45	0.1018	0.1173	0.1299	0.1444
90	0.1065	0.1237	0.1371	0.1536

B. Internal Bus B Fault

If an A-phase ground fault happens on internal bus B, the protective device detects a 'negative' fault direction. When R_f = 50Ω, θ_f = 45°, the *NWEE* at bus B fault is shown in Fig. 8. It is easy to see that at the moment of fault, *NWEE* increases steeply to more than 35, which indicates that there is a fault occurring in the system, and the fault characteristics are obvious.

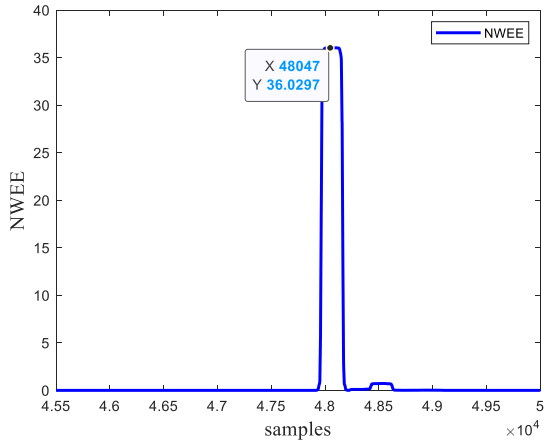

Fig. 8. *NWEE* for bus B fault.

When bus B is faulty under different fault condition attributes, the *NWEE* is displayed in TABLE III. Analyzing the data of Table III, *NWEE* is in the range of [5.8249, 75.3096] and the maximum value is 13 times of the minimum value.

TABLE III
NWEE FOR BUS B FAULT

θ_f(°)	R_f(Ω)			
	0	50	100	250
1	43.7340	19.0767	11.4688	5.8249
3	66.0062	29.7734	18.1189	9.3462
5	75.3096	34.4550	21.1113	10.9878
45	72.4918	36.0297	23.0929	12.7261
90	71.9941	36.6656	23.8005	13.3164

C. Internal Line BC Fault

When a phase A ground fault is at the point F_3 of internal line BC, the current traveling wave propagates directly to the protective installation. The protection device detects the fault direction as 'negative'. The distance L2 from the point F_3 to bus B is 1km and 179km respectively. When point F_3 is faulty, the *NWEE* with R_f = 50Ω and θ_f =45° is shown in Fig. 9. At the moment of fault, the *NWEE* of proximal faults increases steeply by more than 70 and the *NWEE* of remote fault increases steeply by more than 10. They indicate that a fault has occurred. The fault characteristics are obvious.

The *NWEE* for line BC fault under different fault condition attributes is shown in TABLE IV. For L2=1km, *NWEE* is at [39.0123, 90.8629] and the maximum value is 2.3 times the minimum value. For L2=179km, *NWEE* is at [6.1213, 17.9482] and the maximum value is 2.9 times the minimum value. A comparative analyzing the data in TABLE IV and TABLE I reveals that, compared with the original fault feature *WEE*, the synthetic fault feature *NWEE*, which if fused fault attribute information, is significantly less affected by fault condition attributes. This shows that the algorithm can overcome the adverse effects of fault condition attributes. When line BC occurs fault, *NWEE* of all faults is at [6.1213, 90.8629].

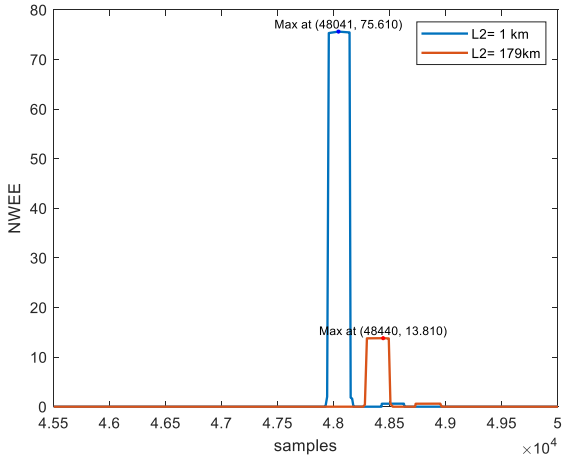

Fig. 9. *NWEE* for line BC fault.

TABLE IV
NWEE FOR F_3 POINT FAULT

θ_f(°)	R_f(Ω)			
	0	50	100	250
	L2=1km			
1	39.0123	41.5794	43.8021	44.9920
3	61.0875	65.4966	69.3075	71.8430
5	70.2464	75.6032	80.2283	83.6375
45	68.2551	75.6139	81.9318	88.9546
90	67.8199	75.8253	82.6901	90.8629
	L2=179km			
1	6.1213	7.0906	7.8478	8.6669
5	9.6203	11.1888	12.4245	13.8203
45	11.1463	12.9964	14.4614	16.1575
90	11.6373	13.8135	15.5908	17.9482

D. Bus C Fault

If an A-phase ground fault happens at the internal bus C, the protective device detects a 'negative' fault direction. When bus C is faulted, the *NWEE* with R_f = 50Ω and θ_f = 45° is shown in Fig. 10. It is easy to see that at the moment of the fault. The *NWEE* increases steeply to more than 6, which indicates that there is a fault and the fault is characterized prominently.

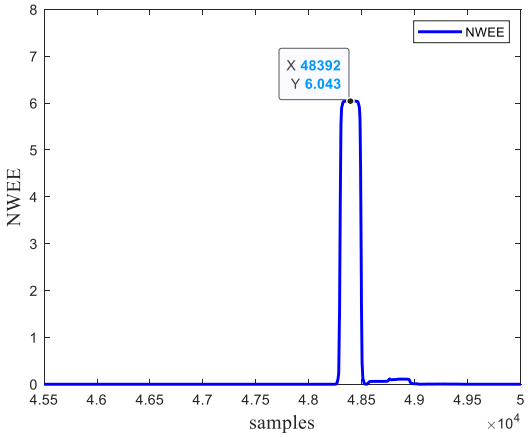

Fig. 10. *NWEE* for bus C fault.

The *NWEE* at bus C fault with different fault condition attributes is shown in TABLE V. The *NWEE* is in [0.8955, 10.2680] and the maximum value is 11 times of the minimum value.

TABLE V
NWEE FOR BUS C FAULT

θ_f(°)	R_f(Ω)			
	0	50	100	250
1	5.2038	2.7939	1.7423	0.8955
3	8.3357	4.6324	2.9237	1.5248
5	9.6920	5.4532	3.4629	1.8207
45	10.1132	6.0430	3.9841	2.1992
90	10.2680	6.2345	4.1517	2.3202

E. External Line CD Failure

When a phase A ground fault happens at point the F_5 of external line CD, fault current traveling wave disseminates through bus C to the Relay. The Relay detects the fault direction as 'negative'. The distance L3 from the point F_5 of line CD to bus C is 1km and 174km respectively. When point F_5 fails, the *NWEE* with $R_f = 50\Omega$ and $\theta_f = 45°$ is shown in Fig. 11. At the moment of fault, the *NWEE* increases steeply, which indicates that there is a fault occurring in the system, and the fault characteristics are obvious.

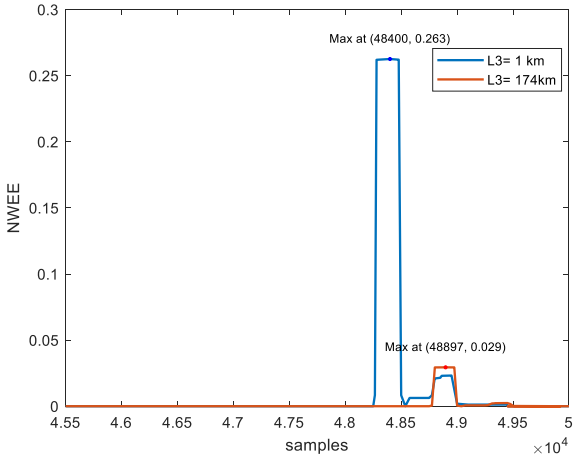

Fig. 11. *NWEE* for line CD fault.

TABLE VI
NWEE FOR F_5 POINT FAULT

θ_f(°)	R_f(Ω)			
	0	50	100	250
		L3=1km		
1	0.0971	0.1138	0.1268	0.1410
3	0.1558	0.1831	0.2043	0.2281
5	0.1839	0.2165	0.2419	0.2708
45	0.2212	0.2626	0.2955	0.3357
90	0.2337	0.2781	0.3135	0.3574
		L3=174km		
1	0.0119	0.0127	0.0152	0.0168
3	0.0174	0.0205	0.0229	0.0256
5	0.0206	0.0242	0.0271	0.0303
45	0.0248	0.0294	0.0331	0.0376
90	0.0252	0.0331	0.0351	0.0391

When line CD is faulted, *NWEE* for different fault condition attributes is shown in TABLE VI. When L3=1km, *NWEE* is [0.0971, 0.3574], and the maximum value is 3.7 times of the minimum value. When L3=174km, *NWEE* is [0.0119, 0.0391], and the maximum value is 3.3 times of the minimum value. Comparison of data in TABLE VI and TABLE I, it can be seen that the synthetic fault feature *NWEE*, which if fused fault attribute information, is significantly less affected by fault condition attributes than the original fault feature *WEE*. This shows that the algorithm can overcome the adverse effects of fault condition attributes. When line CD is faulted, *NWEE* of all failures is at [0.0119, 0.3574].

F. Simulation Comprehensive Analysis and Action Value Setting

After comprehensive analysis of all fault simulation cases from TABLE II to TABLE VI, we draw conclusions as following.

1) If the internal line BC or bus bar B is faulted, *NWEE* is greater than 5.8; Bus B is faulty and the fault direction is positive; Line BC is faulty and the fault direction is negative.
2) When external line AB or line CD is faulty, *NWEE* is less than 1.2239.
3) When bus C fails, *NWEE* is at [0.8955, 10.2680].

From these data, it can be seen that the *NWEE* when the internal line BC or bus B is faulty is significantly different from the *NWEE* when the external line AB or line CD is faulty. According to NWEE, the faults in and out of the area can be accurately judged. The *NWEE* of bus C fault intersects with the *NWEE* of line BC and bus B fault, and these faults cannot be distinguished by *NWEE*. However, from the point of view of tripping circuit breaker by protection action, circuit breaker CB1 should also be tripped when bus C is faulted. Therefore, the inability to distinguish a fault between bus C and line BC does not affect the correct tripping of circuit breaker CB1 by this protection algorithm.

In summary, considering the protection sensitivity requirements, the protection criteria are set as follows.

1) When *NWEE* >3 and the fault direction is 'positive', judge it as bus B fault and switch off breaker CB1.
2) When *NWEE* >3 and the fault direction is 'negative', judge it as line BC fault, and switch off breaker CB1.
3) When *NWEE*⩽3, judge it as out-of-area fault, circuit breaker CB1 will not operate.

V. Conclusion

The two fault condition attributes were found to be the two key factors affecting the solution of the problem that conventional single-ended transient protection cannot distinguish the fault at the end of the line from the fault at first end of the neighboring line, as well as the problem of insufficient sensitivity and reliability in the case of weak faults. The intrinsic relation between wavelet energy entropy and fault condition attributes is mined, and the synthetic fault characteristics are obtained by fusion of wavelet energy entropy and fault condition attributes. The two-dimensional space of original fault characteristics with only time attributes is sublimated into a four-dimensional space of

synthetic fault characteristics with time attributes and two fault condition attributes, which overcomes the adverse effect of fault condition attributes. The algorithm solves 42.2% of cross data, 41.6% of mis-operation or 8.9% of refusal operation. It protects a line and a bus at the same time. A large number of ATP-Draw simulation experiments verify the dependability and accuracy of the proposed algorithm.

REFERENCES

[1] J. Sonang, X. Y. Deng, A. Kader, and R. Li, "New Principle of Bus Protection Based on Integrated Impedance," *Power System Protection and Control*, vol. 38, no. 18, pp. 1-7, Sep. 2010.

[2] R. L. da S. França, F. C. da S. Júnior, T. R. Honorato, J. P. G. Ribeiro, F. B. Costa, F. V. Lopes, and K. Strunz, "Traveling Wave-Based Transmission Line Earth Fault Distance Protection," *IEEE Transactions on Power Delivery*, vol. 36, no. 2, pp. 544–553, Apr. 2021.

[3] Yin-Yin Bao, Yu Liu, Jie-Sheng Wang, and Ming-Wei Wang, "GMDH-type Neural Network Based Short-term Load Forecasting Method in Power System," IAENG International Journal of Computer Science, vol. 50, no. 4, pp. 1194-1201, 2023.

[4] Li Dongping, Yang Yingchun, Shen Shikai, He Jun, Shen Haoru, Yue Qiang, Hong Sunyan, and Deng Fei, "Research on Fault Diagnosis based on Improved Generative Adversarial Network under Small Samples," IAENG International Journal of Computer Science, vol. 50, no. 1, pp. 7-13, 2023.

[5] K. M. Silva, W. L. A. Neves, and B. A. Souza, "Distance protection using a wavelet-based filtering algorithm," *Electric Power Systems Research*, vol. 80, no. 1, pp. 84–90, Jan. 2010.

[6] F. A. Albasri, T. S. Sidhu, and R. K. Varma, "Performance Comparison of Distance Protection Schemes for Shunt-FACTS Compensated Transmission Lines," *IEEE Transactions on Power Delivery*, vol. 22, no. 4, pp. 2116–2125, Oct. 2007.

[7] K. Nayak, S. Jena, and A. K. Pradhan, "Travelling Wave Based Directional Relaying Without Using Voltage Transients," *Transactions on Power Delivery*, vol. 36, no. 5, pp. 3274–3277, Oct. 2021.

[8] F. Jiang, Z. Q. Bo, M. A. Redfern, G. Weller, Z. Chen, and X. Dong, "Application of wavelet transform in transient protection-case study: busbar protection," *in 2001 Seventh International Conference on Developments in Power System Protection* (*IE*E), Apr. 2001.

[9] K. Jia, Z. Yang, L. Zheng, Z. Zhu, and T. Bi, "Spearman Correlation-Based Pilot Protection for Transmission Line Connected to PMSGs and DFIGs," *IEEE Transactions on Industrial Informatics*., vol. 17, no. 7, pp. 4532–4544, Jul. 2021.

[10] A. Lei, X. Dong, and V. Terzija, "An Ultra-High-Speed Directional Relay Based on Correlation of Incremental Quantities," *IEEE Transactions on Power Delivery*, vol. 33, no. 6, pp. 2726–2735, Dec. 2018.

[11] X. Dong, S. Luo, S. Shi, B. Wang, S. Wang, L. Ren, and F. Xu, "Implementation and application of practical traveling-wave-based directional protection in UHV transmission lines," *in 2016 IEEE Power and Energy Society General Meeting* (*PESGM*), Boston, MA, USA: IEEE, Jul. 2016, pp. 1–1.

[12] K. Nayak, S. Jena, and A. K. Pradhan, "Travelling Wave Based Directional Relaying Without Using Voltage Transients," *IEEE Transactions on Power Delivery*, vol. 36, no. 5, pp. 3274–3277, Oct. 2021.

[13] S. Jena and A. K. Pradhan, "Transmission Line Protection Using Decaying DC Information in Fault Current," *IEEE Transactions on Industrial Informatics*, vol. 19, no. 7, pp. 8452-8461, July 2023.

[14] Z. Guo, J. Yao, and Z. Tan, "Hilbert–Huang transform-based transient busbar protection algorithm", *IET Generation, Transmission & Distribution*, vol. 9, no. 14, pp. 2032–2039, 2015.

[15] Z. Shi, C. Lu, Y. Jiang, X. Ding, H. Gao, and Z. Wang, "Transient Protection of EHV AC Line Based on Wavelet Packet Entropy," *in 2022 International Conference on Power Energy Systems and Applications* (*ICOPESA*), Singapore, Singapore: IEEE, Feb. 2022, pp. 206–212.

[16] Z Lu, Z Wang, W Xu, and J Liang, "Series Protection of UPFC Line Based on Transient Spectral Information Associated with Busbar," *Automation of Electric Power Systems*, vol. 44, no. 2, pp. 139–146, 2020.

[17] N. Zhang and M. Kezunovic, "Transmission Line Boundary Protection Using Wavelet Transform and Neural Network," *IEEE Transactions on Power Delivery*, vol. 22, no. 2, pp. 859-869, April 2007.

[18] Z. Guo, J. Yao, and T. Kang, "An Ultra-High-Speed Directional Protection Method for Transmission Lines," *Transactions of China Electrotechnical Society*, vol. 31, no. 22, pp. 168–177, 2016.

[19] N. Kondrath and M. K. Kazimierczuk, "Bandwidth of Current Transformers," *IEEE Trans. Instrum. Meas*., vol. 58, no. 6, pp. 2008–2016, Jun. 2009.

[20] Z. Chang, J. Yan, C. Zhang and G. Song," A high speed and sensitive protection for distribution network with DGs using ferrite rings as line boundary," *IET Gener. Transm. Distrib.*, vol. 18, pp. 1611–1623, 2024.

[21] Len Gelman, and Tejas H. Patel, "Novel Intelligent Data Processing Technology, based on Nonstationary Nonlinear Wavelet Bispectrum, for Vibration Fault Diagnosis," IAENG International Journal of Computer Science, vol. 50, no. 1, pp. 1-6, 2023.

[22] Karim M. Aljebory, Yashar M. Jwmah, and Thabit S. Mohammed, "Classification of EMG Signals: Using DWT Features and ANN Classifier," IAENG International Journal of Computer Science, vol. 51, no. 1, pp. 23-31, 2024.

[23] I. F. Prado, F. B. Costa, K. M. Silva, R. P. Medeiros and B. A. Mork, "High-Frequency-Based Transmission Line Percentage Differential Protection With Traveling Wave Alignment," *IEEE Access*, vol. 12, pp. 129404-129416, 2024.

[24] Y. Kong, B. Zhang and Z. Hao, "Study of Ultra-High-Speed Protection of Transmission Lines Using a Directional Comparison Scheme of Transient Energy," *IEEE Transactions on Power Delivery*, vol. 30, no. 3, pp. 1317-1322, June 2015.

[25] G. Zou and H. Gao, "A Traveling-Wave-Based Amplitude Integral Busbar Protection Technique," *IEEE Transactions on Power Delivery*, vol. 27, no. 2, pp. 602–609, Apr. 2012.